Journal of Magnetism and Magnetic Materials 326 (2013) 138–146

Contents lists available at SciVerse ScienceDirect

Journal of Magnetism and Magnetic Materials

journal homepage: www.elsevier.com/locate/jmmm

Effect of thermal fluctuations in FMR experiments in uniaxial magnetic nanoparticles: Blocked vs. superparamagnetic regimes

E. De Biasi *, E. Lima Jr., C.A. Ramos, A. Butera, R.D. Zysler

Centro Atómco Bariloche, Av. Bustillo 9500, CP 8400 S.C. de Bariloche, RN, Argentina

ARTICLE INFO

Article history:
Received 22 March 2012
Received in revised form
22 August 2012
Available online 7 September 2012

Keywords:
Ferromagnetic resonance
Thermal fluctuations
Blocking
Superparamagnetism

ABSTRACT

We present ferromagnetic resonance (FMR) experiments on two low-interacting nanoparticle systems: Fe_3O_4 and $CoFe_2O_4$ corresponding to low- and high-anisotropy cases, respectively. The spectra have been interpreted in terms of a phenomenological model which applies to the FMR of nanoparticles. The model includes the effect of thermal fluctuations in the FMR covering the range from the superparamagnetic (low-anisotropy-high-temperature) regime to the high-anisotropy-low-temperature situation. We have been able to explain several simultaneous features observed in the FMR spectra of a system of anisotropic nanoparticles when lowering the temperature that include: a decrease of the resonance field with a simultaneous linewidth increase and intensity reduction. These effects had been previously attributed to the existence of a "blocking-temperature" in the FMR. Our interpretation, however, shows that in a magnetic system with easy axes this FMR response originates in the temperature dependence of the dispersion relation. Also, applying the present model to the FMR within the hysteresis cycle it is possible to reproduce the irreversibilities occurring in the resonance spectra. Comparison of FMR and magnetization measurements show that the characteristic FMR time is not related to the inverse microwave frequency.

1. Introduction

Ferromagnetic resonance is one of the most widely used techniques for determining many physical characteristics in magnetic systems: magnitude and type of anisotropy, *g*-factor, relaxation, and transition temperatures are among the most commonly reported [1]. This technique has been extensively used in the study of bulk materials, thin films [2–5], nanoparticles (NP), nanotubes, nanowires and other nanostructured systems [6–15]. At the nanoscale level thermal fluctuations (TFs) must be considered [16], especially in NP. In fact, it is well known that a system of NP can show very different regimes depending on the temperature (T) and the experimental time window (τ_m) while remaining in a ferromagnetic state. For a given magnetic anisotropy, the NP can be observed in a superparamagnetic (SPM) or blocked regime depending on T, the magnetic field, H, and τ_m [17].

Usually the literature treats FMR experiments in the SPM and blocked-regimes separately. At low T the system can be treated as a standard ferromagnet, and the SPM regime describes the low anisotropy-field approximation [16,18–22]. Nevertheless, we are not aware of published works in which the "transition" between the above mentioned regimes is completely described by a single model. In several works of FMR on NP it was assumed that the microwave frequency defines τ_m and thus separates the regimes: either SPM or blocked [23–29]. This assumption has led some authors to consider extremely small values for the intrinsic relaxation time (τ_0) to explain the SPM behavior observed at room temperature when measuring at typical microwave frequencies (10 GHz) [30,31]. In addition, it is not straightforward to distinguish between SPM- or blocked-regimes from standard FMR experiments. Understanding the blocked-regime response has led to recent contributions (De La Torre *et al.* [32]) where reversal-curve FMR of nanowire arrays has been used as a key element of microwave devices.

In this work we present FMR and magnetization measurements on low- and high-anisotropy NP dispersed in a non-magnetic matrix. We compare the FMR experiments with a model that takes into account the effects of magnetic anisotropy and thermal fluctuations on the spectra. The main contribution of this work is to introduce a phenomenological model describing the FMR experiments in a wide range of temperatures, anisotropies, and applied fields.

The work is organized as follows: in Section 2 we review the concepts of superparamagnetic/blocked regimes and describe the ferromagnetic resonance equations that apply to a system with a bi-stable uniaxial anisotropy. Section 3 presents the experimental results in Fe_3O_4 and $CoFe_2O_4$ nanoparticles. Section 4 describes a model that takes into account the thermal fluctuations in the FMR

* Corresponding author. Tel.: +54 294 4445158.
E-mail addresses: debiasiem@gmail.com, debiasi@cab.cnea.gov.ar (E. De Biasi).

0304-8853/$ - see front matter © 2012 Elsevier B.V. All rights reserved.
http://dx.doi.org/10.1016/j.jmmm.2012.08.046

measurements. Section 5 presents numerical simulations to compare with our experimental results, and we give the conclusions in Section 6.

2. Magnetic behavior of nanoparticles and ferromagnetic resonance in uniaxial systems

2.1. Superparamagnetic and blocked regimes

By superparamagnetic [17] and blocked-regimes we refer to different ways in which single-domain magnetic NP can be observed, while remaining always in the ferromagnetic state. The blocked regime is out of thermal equilibrium while the SPM is not. By thermal equilibrium we mean that the magnetization orientation can explore all (θ,ϕ) values with some probability. When a single-domain NP system is in the SPM regime its behavior is reversible and, for each value of T and H there is a single magnetization value, independent of the magnetic history of the system. On the contrary, a system in the blocked-regime will show hysteresis: its magnetization will depend on H, T, and its previous history. The relation between the magnetic relaxation time, τ, and the measuring time (or time-window), τ_m, will establish if the system is in one regime or the other. In magnetization measurements, τ_m is the time related to the measuring process. The relaxation time, τ, is associated with the time required by the magnetization to go from an energy minimum to the other. In a single-domain, in which coherent rotation is assumed, the time to overcome the energy barrier $\Delta E_{0,1}$ (Fig. 1) is given by the Arrhenius law [17]:

$$\tau_{+,-} = \tau_0 e^{\Delta E_{0,1}/k_B T} \tag{1}$$

where τ_0 is the characteristic relaxation time when the energy barrier is much smaller than the thermal energy ($\Delta E \ll k_B T$). In Fig. 1 we present an energy double well associated with a uniaxial anisotropy for $H=0$ (dash-line) and H parallel to the easy axis (solid line). The time τ is given by:

$$\frac{1}{\tau} = \frac{1}{\tau_+} + \frac{1}{\tau_-} \tag{2}$$

which depends on the H value. When $\tau < \tau_m$ the magnetic moment will reach equilibrium within the measuring time (SPM regime), while if $\tau > \tau_m$ the magnetic moment will not be able to cross the energy barrier during the measuring time and therefore will be in the blocked regime.

The SPM regime resembles a paramagnetic state. The blocked regime can be more easily identified with a standard ferromagnetic behavior, although the TFs produce small perturbations that need to be considered [16].

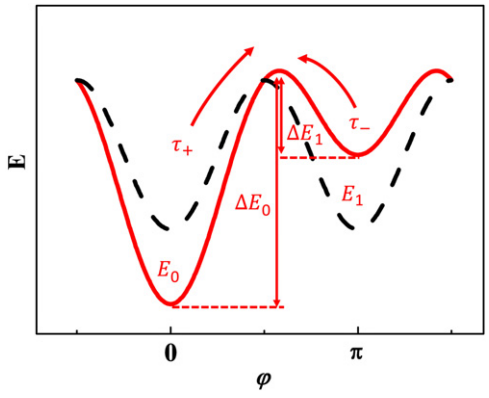

Fig. 1. Schematic energy minima representation as function of the magnetization orientation. Dashed and continuous lines correspond to $H=0$ and $H=H_A/2$ half the anisotropy field (see text). In both cases the field is applied along the easy axis. $\tau_\pm$ are the times associated to overcome the $\Delta E_{0,1}$ energy barriers.

2.2. Ferromagnetic resonance in uniaxial anisotropy samples.

In ferromagnetic resonance, energy is absorbed from the microwave excitation, while the magnetic moment precesses around the energy minimum. Varying H changes the curvature of the energy minimum (Fig. 1) and, consequently, the magnetic moment precession frequency of each minimum is modified. When the magnetization precession and microwave frequencies coincide, energy can be absorbed from the electromagnetic field reaching the resonance condition. The energy absorbed is released to the lattice. Note that in our FMR experiment, the microwave fields ($h_{rf}\sim$ 0.1 Oe) are negligible when compared with typical anisotropy fields [17] ($\sim$1000 Oe). As a consequence, microwave excitation can produce changes in the double well shape of only $\sim 1/10^4$, aside from a small periodic perturbation of the magnetic moment orientation around the given minimum. The strong spin–lattice relaxation does not allow for significant departures of the magnetic moment from the equilibrium orientation [33], contrary to what can be done in nuclear magnetic resonance, where the spin–lattice relaxation is governed by weak nuclear dipole–dipole interactions (at least 10^6 times smaller than in FMR). For this reason the microwave excitation used in FMR does not play any significant role in reorienting the magnetic moment from a minimum to the other. Thus, the double-well relaxation time τ (Eq. 2) is not related or affected by the microwave frequency.

The time evolution of the magnetic moment $\vec{\mu}$ is given by [19]:

$$\frac{d\vec{\mu}}{dt} = -\gamma \vec{\mu} \times \vec{H}_T + \alpha \frac{\gamma}{\mu} \vec{\mu} \times (\vec{\mu} \times \vec{H}_T) \tag{3}$$

where γ is the gyromagnetic factor, α is the phenomenological damping constant, and $\vec{H}_T = -\vec{\nabla}_\mu E$ is the energy gradient along the magnetization components. To describe the ferromagnetic resonance, $E(\theta,\varphi)$ is expanded to second order in θ and φ around the minima. In this way, linearizing Eq. (3) in the microwave field components, we obtain the magnetic susceptibility whose imaginary component is related to the energy absorption [34,35]. Then, the resonance angular frequency, ω_r, and the absorption angular frequency width, $\Delta\omega$, are given by:

$$\frac{\omega_r}{\gamma} = \frac{1}{\mu \sin\theta} \sqrt{E_{\theta\theta} E_{\varphi\varphi} - E_{\theta\varphi}^2}\Big|_{\theta_i^e,\varphi_i^e} + O(\alpha^2) \tag{4a}$$

and

$$\frac{\Delta\omega}{\gamma} = \frac{\alpha}{\mu}\left[E_{\theta\theta} + \frac{E_{\varphi\varphi}}{\sin^2\theta}\right]\Big|_{\theta_i^e,\varphi_i^e} \tag{4b}$$

where $E_{\theta\theta}$, $E_{\varphi\varphi}$, and $E_{\theta\varphi}$ are the second derivatives of the energy with respect to the magnetization orientation angles (θ,φ), evaluated at the equilibrium positions (θ_i^e,φ_i^e) and the subindex $i=0$, 1 refers to the minima of Fig. 1.

From a typical FMR linewidth of 100 Oe (Eq. 4b), we estimate the magnetization decays into the local equilibrium direction in $\sim 10^{-9}$ s. This damping time is not related to the relaxation between energy minima of Fig. 1, given by τ (Eq. 2).

Eq. (4a) is known as the Smit–Beljers dispersion equation. For the case of a uniaxial nanoparticle this equation can be explicitly written as:

$$\left(\frac{\omega_r}{\gamma}\right) = [H\cos\varphi + H_A\cos^2(\varphi_n-\varphi)][H\cos\varphi + H_A\cos 2(\varphi_n-\varphi)]^{1/2}\Big|_{\varphi=\varphi_i^e} \tag{5}$$

where $H_A = 2K/M$ is the anisotropy field, K the anisotropy constant and φ is evaluated at the magnetization equilibrium direction(s), φ_i^e (see Fig. 1). The right-hand member of Eq. 5 is plotted as a function of H in Fig. 2. The field at which this curve intercepts the value $H_0 = \omega_0/\gamma$ is the resonance field associated with the

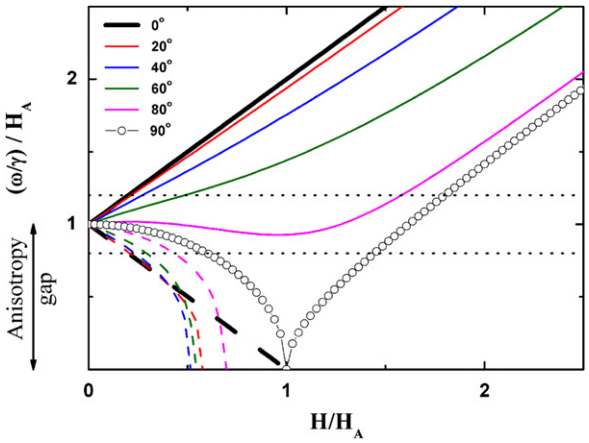

Fig. 2. Dispersion relation as function of H for several values of φ_n, the angle between the field and the easy axis. Continue and dashed lines correspond to E_0 and E_1 energy minima respectively.

minimum in question ($i=0$ or 1). In Fig. 2 we plot the dispersion relation for different orientations of H with respect to the easy axis. Solid lines correspond to the E_0 minimum and the dashed-lines to the other energy minimum, E_1 (Fig. 1). The curve with circles corresponds to the perpendicular orientation. The horizontal dotted-line corresponds to H_0/H_A. When $H_A > H_0$ (lower horizontal dashed-line) the system does not reach the resonance condition associated to the E_0 minimum, except for orientations very close to the perpendicular condition. It is customary to refer to this gap in the dispersion relation as the anisotropy gap of the system. On the contrary, the curve associated with the E_1 local minimum will cross the dispersion relation for all angles (dashed lines in Fig. 2).

A simple case is obtained when H is applied along the easy axis:

$$\frac{\omega_r^i}{\gamma} = (H_A \pm H) \tag{6}$$

where the "+" and "−" signs apply for $\varphi_0^e = 0$, and $\varphi_1^e = \pi$ respectively (Fig. 1). The straight lines derived from Eq. 6 are plotted as thick lines in Fig. 2. If we consider the linewidth, power from the microwave field will be absorbed in the field region:

$$\frac{\omega_r}{\gamma} \pm \frac{\Delta\omega}{\gamma} \approx H_0 \tag{7}$$

Performing experiments at a higher microwave frequencies generally implies achieving the resonance condition (Eq. 4a) at a higher field, which leads to a *single* energy minimum for $H > H_A$. The only region where the FMR response will depend on the field history is that for which $H < H_{irr}$ (i.e. the lowest H at which the energy has only one minimum, Fig. 1) and Eq. (7) applies. As we will show in the experimental section, the value H_{irr} obtained from magnetization and FMR measurements are very similar, thus, indicating that the characteristic time of the FMR experiment is related to the sweeping time, as the magnetization follows very closely the equilibrium direction of each minimum as long as $H < H_{irr}$.

To study its FMR response we have chosen two samples (and particular temperatures) in which the anisotropy field is lower or higher than H_0. The first system consists of dispersed Fe_3O_4 NP at low temperature and the second is a collection of $CoFe_2O_4$ NP oriented and dispersed NP in a non-magnetic matrix. In both cases H_0 corresponds to field for X-band frequency (9.45 GHz)

3. Experimental results.

3.1. Samples and experimental details

Fe_3O_4 and $CoFe_2O_4$ NP were used in this work in order to test the FMR response in two limits, low and high anisotropy. Fe_3O_4 has a room temperature anisotropy constant [36] $K \sim 4.1 \times 10^5$ erg/cm^3, while that of $CoFe_2O_4$ is $K \sim 1.8$–3.0×10^6 erg/cm^3 (see Ref. [37]). Considering these values we estimate $H_A = 1.6$ kOe and $H_A = 10$ kOe for Fe_3O_4 and $CoFe_2O_4$ NPs respectively.

Fe_3O_4 NP were obtained by means of thermal decomposition of Fe^{3+}acetylacetonate in the presence of oleic acid and using trioctylamine as solvent. The synthesis was performed at reflux condition with N_2 during 30 min. After that, the NP were precipitated by adding ethanol followed by centrifugation. The hydrophilic character of the NP were produced by adding tetramethylammoniun 11-aminodecanoic salt (10 mMol:1 mMol of NPs) in a solution of dicloromethane containing the NP (0.1 wt%). $CoFe_2O_4$ NP were synthesized by milling cobalt ferrite powder in water/oleic acid solution (50–50%) and, after washing the product with water, a ferrofluid NPs/water suspension was obtained.

Transmission electron microscopy (TEM) images of the Fe_3O_4 NP show high crystallinity particles with an average size of 20 nm (Fig. 3). Similarly TEM images of the $CoFe_2O_4$ NP show a mean size of 8 nm (Fig. 4).

Finally, in order to obtain textured samples with low interacting NPs, the particles were dispersed in acrylamide (1% $w_{particles}/w_{polymer}$) and the polymerization took effect under an applied magnetic field, $H = 20$ kOe.

The magnetization measurements were performed in a commercial Lakeshore VSM and a MPMS SQUID magnetometer.

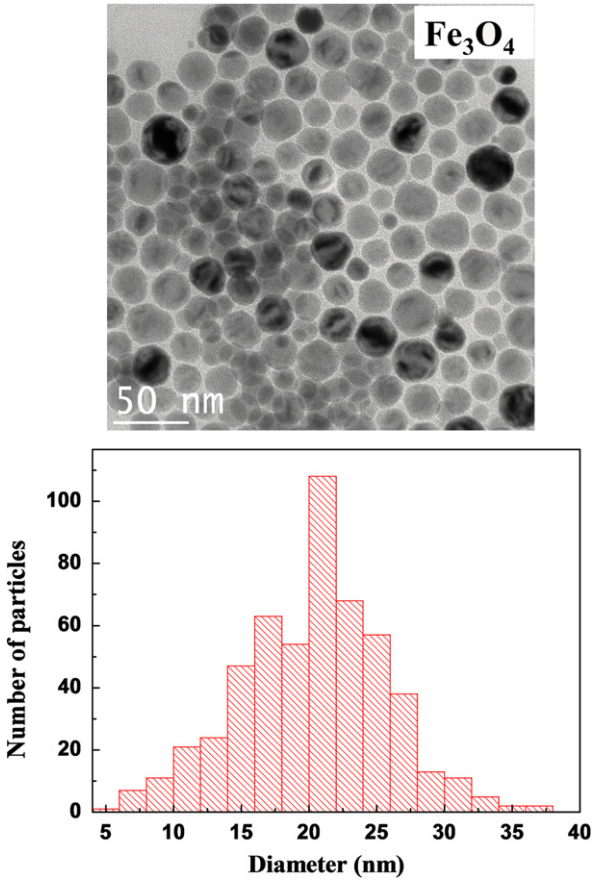

Fig. 3. Top: TEM image of Fe_3O_4 NPs. Bottom: particle diameter histogram.

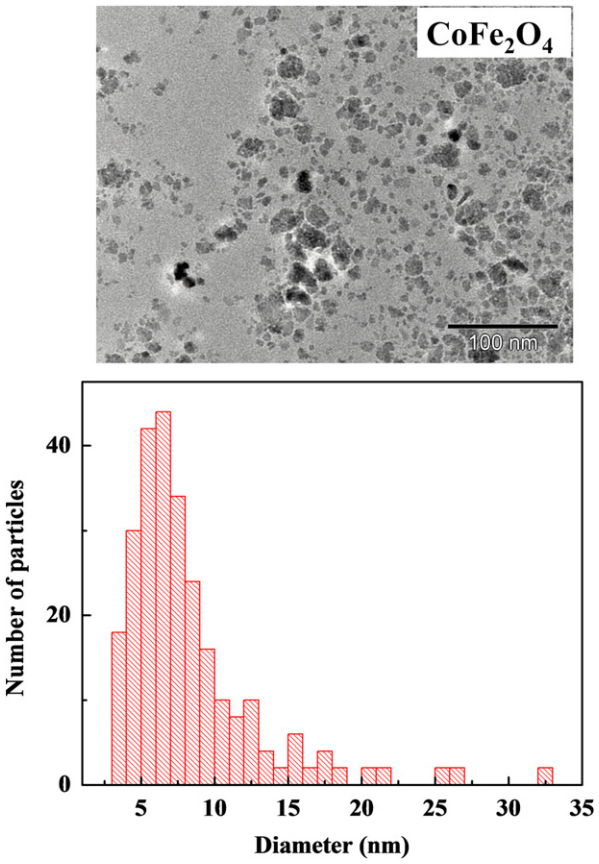

Fig. 4. Top: TEM image of $CoFe_2O_4$ NPs. Bottom: particle diameter histogram.

The FMR experiments were performed in an ESP300 Bruker spectrometer operating at X Band.

3.2. Magnetization measurements

Fig. 5 shows the Field Cooling (FC) and Zero Field Cooling (ZFC) magnetization measurements normalized by M_{FC} (5 K) for comparison. There is a clear difference in the magnetic behavior observed in both samples due to the different magnetic anisotropy. The T at which the Fe_3O_4 sample reaches the M(ZFC) maximum and its irreversibility temperature (the lowest T at which FC and ZFC magnetization merges) are both lower than those corresponding to the $CoFe_2O_4$ sample, in which the FC and ZFC data indicate that the system remains blocked for $H=100$ Oe up to room T. This fact corroborates the different anisotropy strength of the Fe_3O_4 and $CoFe_2O_4$ samples.

In Fig. 6 we show hysteresis loops performed in samples of Fe_3O_4 (5 K) and $CoFe_2O_4$ (300 K). H_{irr} is about 1.5 ± 0.1 kOe for both samples.

In spite of having a similar H_{irr}, the FMR response of both samples at these particular temperatures is significantly different.

3.3. FMR measurements

We show in Fig. 7 the FMR spectra of the Fe_3O_4 sample. At higher temperatures the spectra are symmetrical, and when T is decreased the linewidth increases and the spectra lose their symmetry. These effects are due to the increase in the effective anisotropy field [16,20,23] when T is lowered. At $T=6$ K the anisotropy distribution becomes relevant and the lineshape is distorted [38]. The FMR signal of $CoFe_2O_4$ vanishes below room temperature.

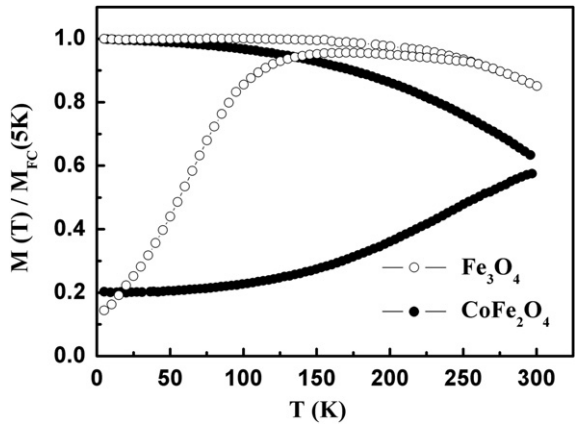

Fig. 5. FC and ZFC magnetization measurement on samples of Fe_3O_4 and $CoFe_2O_4$ ($H=100$ Oe).

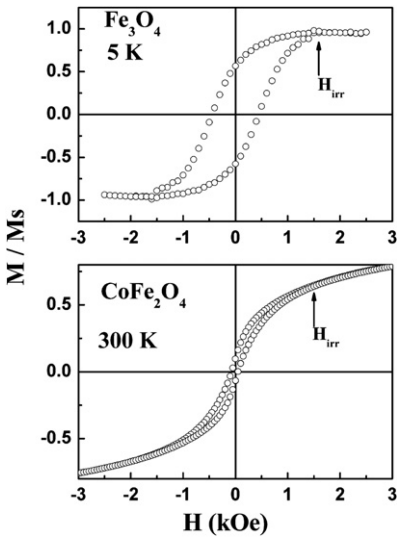

Fig. 6. Hysteresis loops of samples Fe_3O_4 (5 K) and $CoFe_2O_4$ (300K). The curves are normalized to the saturation value.

Fig. 8 presents the FMR data measured at X band (9.45 GHz) on the Fe_3O_4 and $CoFe_2O_4$ NP systems recorded at 5 K and 300 K, respectively. These particular cases were chosen in order to observe the effect of the proximity of the anisotropy field gap, below and above H_0. The narrow signal observed at $g \sim 2.00$ in the latter case corresponds to a DPPH marker used to verify the correct phase of the spectrum. The protocol applied to measure the effect of magnetic irreversibility in the FMR spectra (similar to the magnetic hysteresis cycle) is as follows: (1) we magnetize the system along the easy axis with $H > H_{irr}$. Then we set $H=0$ and measure the FMR DM (Direct Magnetization) spectrum; (2) subsequently we set $H=0$, rotate the sample by 180°, and take a new FMR IM (Inversed Magnetization) spectrum. The magnetic field region where the DM and IM spectra are significantly different indicates the manifestation in the FMR experiment of a blocked regime.

In the low anisotropy case (Fe_3O_4 NPs), the DM shows absorption at $H=0$ corresponding to a wide resonance line centered at $H \approx 2.6$ kOe, and the initial IM (for $H < H_{irr}$) resembles a "tail" coming from negatives fields. The inset in the top panel in Fig. 8 shows a FMR measurement at $T=105$ K acquired with the same protocol. in which we do not observe significant differences in the resonance spectra between DM and IM measurements. Note also that lineshapes are more symmetrical than at $T=5$ K.

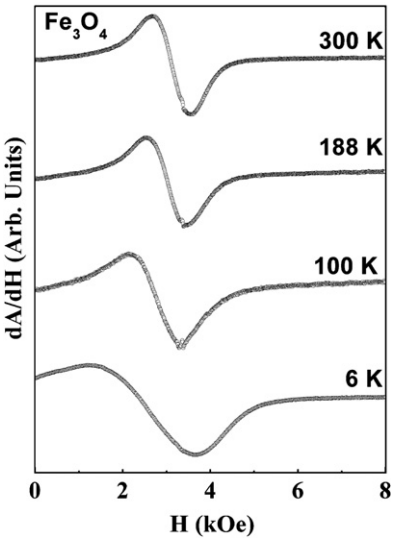

Fig. 7. FMR spectra corresponding to the Fe_3O_4 sample at several temperatures.

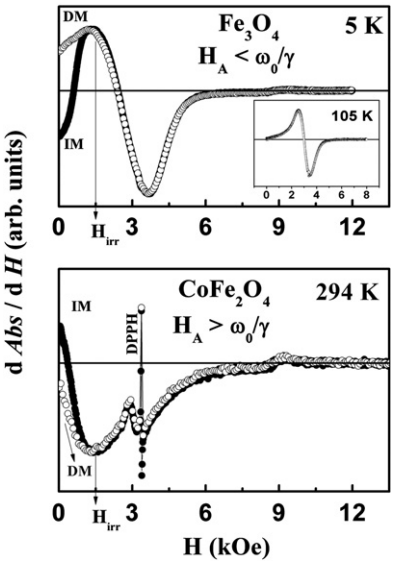

Fig. 8. DM and IM spectra for Fe_3O_4 (top) and $CoFe_2O_4$ (bottom).

Comparison of the irreversibility field, H_{irr}, from the $M(H)$ measurement (Fig. 6) and the irreversibility field observed comparing DM with IM FMR spectra (Fig. 8) show that they are coincident.

4. The model: thermal fluctuations effects on the effective magnetization and anisotropy

Our model assumes a system of identical, non-interacting, and single domain NP in which each particle reverts the magnetization coherently under the influence of an easy axis uniaxial anisotropy. This latter assumption is not essential, but simplifies the theoretical-computational treatment, and does not impose serious restrictions to the real systems, because uniaxial magnetic anisotropy is usually the dominant anisotropy in NPs [17].

The magnetic energy of a single-domain nanoparticle under an external applied field, $\vec{H}$, can be written as [39]:

$$E = -\vec{\mu}\,\vec{H} - KV(\hat{n}\hat{\mu})^2 \tag{8}$$

where $\vec{\mu} = MV\hat{\mu}$ is the magnetic moment pointing along the unit vector $\hat{\mu}$, M is the saturation magnetization, $K > 0$ is the anisotropy constant, V is the particle volume, and $\hat{n}$ is the anisotropy unit vector orientation. Hereafter, we assume that $\vec{H}$ is applied along the x-direction, and $\hat{n}$ lies on the $\theta = \pi/2$ plane, forming an angle φ_n with the x-axis. In this configuration the equilibrium magnetization that minimizes the energy will have a coordinate $\theta^e = \pi/2$.

In order to consider thermal effects on the magnetic moment and anisotropy behaviors, we will correct these quantities (μ and K) considering the thermal fluctuations by means of Statistical Averages on the Energy Space (SAES) using the Boltzmann probability, as was indicated by de Biasi and Devezas [18] in the limit case of $H \gg 2K/M = H_A$. In our model the temperature correction is incorporated by means of SAES, which modifies the effective magnetization and anisotropy using Eq. (8) in the Boltzmann probability. We will refer to M_{eff} and K_{eff} as the thermally corrected magnetic moment and anisotropy respectively. In the case of a uniaxial system described by Eq. (8) there are two minima for $H < H_A$ and a single minimum otherwise.

For a given energy minimum $(\theta_i^e, \varphi_i^e)$ we can associate an effective magnetic field which points along this orientation: $\hat{n}_i^e = (\sin\theta_i^e \cos\varphi_i^e,\ \sin\theta_i^e \sin\varphi_i^e,\ \cos\theta_i^e)$.

It is convenient to find an approximate expression for the local energy minima. The energy landscape in the (θ,ϕ) space can be approximated around the magnetization equilibrium positions where we can consider an effective field $(\vec{H}_{eff})$ is applied. As the magnetization unit vector points along $\hat{M} = (\sin\theta\cos\varphi,\ \sin\theta\sin\varphi,\ \cos\theta)$, then the scalar product with the local equilibrium direction is given by:

$$\hat{\mu}\cdot\hat{n}_i^e = \sin(\theta)\sin(\theta_i^e)\cos(\varphi - \varphi_i^e) + \cos(\theta)\cos(\theta_i^e) \tag{9}$$

The thermal correction of the magnetization fluctuation around its minimum can be calculated as:

$$m_{T,i} = \frac{1}{1-\lambda_{m,i}} \int_{\Omega_i} P_i(\hat{\mu}\cdot\hat{n}_i^e - \lambda_{m,i})\,d\Omega \tag{10}$$

where $P_i = e^{-E_i/k_BT}/Z_i$, $Z_i = \int_{\Omega_i} e^{-E_i/k_BT}\,d\Omega$, and $\lambda_{m,i} = \int_{\Omega_i}(\hat{\mu}\cdot\hat{n}_i^e)\,d\Omega$. The determination of the minima region, Ω_i, has some difficulties, which are treated in the Appendix A. The constant $\lambda_{m,i}$ is defined in order to make $m_{\infty,i} = 0$, and the pre-factor of Eq. (9) is the normalization to obtain $m_{0,i} = 1$ when $T \to 0$.

The effect of TFs on anisotropy can be treated in a similar way, where now the SAES adopts the form:

$$k_{T,i} = \frac{1}{1-\lambda_{K,i}} \int_{\Omega_i} P_i \left[(\hat{\mu}\cdot\hat{n}_i^e)^2 - \lambda_{K,i}\right] d\Omega \tag{11}$$

where, $\lambda_{K,i} = \int_{\Omega_i}(\hat{\mu}\cdot\hat{n}_i^e)^2\,d\Omega$. Expressions (10) and (11) allow the computation of the statistical averages to include TFs into the effective magnetization and anisotropy: $M_{eff,i} = M m_{T,i}$ and $K_{eff,i} = K k_{T,i}$. We have used these values to compute the effective anisotropy field as: $H_{Aeff} = H_A(k_{T,i}/m_{T,i})$. In addition, the extreme cases of low-anisotropy-high-T and high-anisotropy-low-T reproduce the expected results. Effectively, at $T = 0$, both expressions become $m_{T,i} = k_{T,i} = 1$ and, in the low-anisotropy-high-field case only one minimum remains and the Eqs. (10) and (11) yield:

$$m_T = L_1(x) \tag{12a}$$

$$k_T = 1 - (3/x)L_1(x) \equiv L_2(x) \tag{12b}$$

where, $x = \mu H/k_BT$, and $L_1(x) = \coth(x) - 1/x$ is the Langevin function. These results that apply to the SPM regime were obtained by de Biasi and Devezas [18] considering the low anisotropy approximation.

The values of $M_{eff,i}$ and $K_{eff,i}$ replacing the corresponding M and K will be used in the calculation of the microwave absorption contribution of each minimum, as in the "classical" FMR case (Eq. 4a and b).

In the low-anisotropy case there is only one energy minimum determined essentially by H, and its population remains constant. On the other extreme, the high-anisotropy case (in which the effective anisotropy field is comparable or greater than H) involves two issues: the effect of TFs on the magnetization and anisotropy (already given by Eqs. (10) and (11)) and the determination of the energy minima population as function of H, T, τ_m, and the magnetic history. We discuss now the characteristic measuring time in FMR, τ_m.

4.1. The characteristic measuring time in FMR

SQUID and VSM magnetization measurements $M(H)$, were taken in discrete field steps (step-mode) while the FMR spectra were recorded in a quasi-continuous way (sweep-mode). In the $M(H)$ measurements H is changed up to the desired value and M is measured in a time τ_m. In the FMR experiment, the time evolution of the magnetization depends on the sweeping rate. To find an equivalence between the "step" and "sweep" modes we can associate to the "step" mode a sweeping rate $(dH/dt)_{step} = \delta H/\tau_m$, where δH is the field variation between subsequent measurements. The conversion between the "sweep" τ_m and the corresponding "step" τ_m can be expressed as:

$$\tau_m(\text{sweep}) = \frac{(dH/dt)_{step}}{(dH/dt)_{sweep}}\tau_m(\text{step}) \tag{13}$$

where $(dH/dt)_{sweep}$ is the sweep rate in the FMR experiment. This definition of $\tau_m(sweep)$ allows comparison between the step and sweep τ_m. In our case, for the sweeping rate used in Fig. 8, $\tau_m(sweep) \sim 0.13$ s which compares with VSM or SQUID measuring times of $\approx$ 100 s.

Considering the Stoner–Wohlfarth model and Eq. (1) an expression of the irreversibility field as a function of T and τ_m can be given for the case in which H is applied along the easy-axis anisotropy direction [17]:

$$H_{irr} = H_A\left\{1-\left[\frac{k_BT}{KV}\ln(\tau_m/\tau_0)\right]^{1/2}\right\} \tag{14}$$

where $H_A(T=0)$ is the anisotropy field, K is the anisotropy constant and V is the particle volume.

In Table 1 we present the measured values using dc-magnetization measurements (VSM or SQUID) and FMR calculated using Eq. (14). In the last column we added the value calculated for H_{irr} considering $\tau_m = 1/\nu$, with $\nu = 9.45 \times 10^9$ Hz.

Table 1 shows that there is a very good agreement between the measured and calculated values using Eq. (14). If, however, τ_m in FMR were given by $\tau_m = 1/\nu$, the calculated H_{irr} ($CoFe_2O_4$) should be much larger than that observed experimentally, reaffirming the fact that τ_m in FMR is not related to the inverse of the microwave frequency.

The extreme case of a uniaxial single-domain blocked nanometric system occurs in nanowires, in which the FMR signal is clearly observable [40]. In other words, the resonance phenomenon is observed in blocked systems that have a non-reverting magnetic moment.

Table 1
Measured and calculated irreversibility fields in magnetization and FMR using Eq. (14). The number in parenthesis indicates the error in the last digit. The last column corresponds to $\tau_m = 1/\nu$ with $\nu = 9.45$ GHz (*Note*: in this case, the large discrepancy with the experimental value).

Sample	Experimental H_{irr} (kOe)		Calculated H_{irr}		
	$M(H)$	FMR	$M(H)$	FMR	FMR, $\tau m = 1/\nu$
Fe_3O_4 (5 K)	1.5(1)	1.5(3)	1.5	1.5	1.6
$CoFe_2O_4$ (300 K)	1.5(2)	1.5(3)	1.1	1.8	10

4.2. Thermal and temporal evolution of the minima populations.

Now we want to study the energy minima (Eq. (8)) population evolution as a function of H, T, and τ_m. In our model we calculate the contribution of each energy minimum to the FMR absorption and weight this value by the corresponding population. To address this problem, we have used the expression of the temporal evolution of the population minima [16]. Starting from the Master Equation, the time evolution of the population of each minimum, $i=(0, 1)$ as a function of time, P_t^i is given by:

$$P^i_{t+\Delta t} = P^i_t + (P^i_\infty - P^i_t)L \tag{15}$$

where P^i_∞ represents the equilibrium population ($t \to \infty$), P^i_t is the population at time t, Δt is system evolution time (in our case τ_m), and L is given by [16] $L = 1-\exp(-\Delta t/\tau_{rm})$. From Eq. (15) it is possible to obtain the time evolution of $P^i_{t+\Delta t}$ from the initial value P^i_t. The function L is the probability to find the system in the SPM regime. The equilibrium population P^i_∞ of each minimum is obtained by integrating the partition function in a region around the corresponding minimum (as is usually carried out in statistical mechanics). This procedure does not imply additional computational effort because the integrals must be evaluated to calculate Eqs. (10) and (11).

5. Numerical results

In this section we present numerical results applying our model. The physical parameters used in the calculations are: $\tau_m/\tau_0 = 10^9$, (considering [17] $\tau_0 = 10^{-10}$ s), $H_A(T=0) = 3500$ Oe, $M = 400$ emu/cm^3, $\omega_0/\gamma = 3380$ Oe (microwave frequency 9.45 GHz and $g=2$).

Fig. 9 shows the results for $k_{T,i}$ and $m_{T,i}$ as function of H for $\varphi_n = \pi/4$. The open symbols correspond to the lowest minimum equilibrium magnetization angle (going from $\varphi^e_0 = \pi/4$ for $H=0$, to $\varphi^e_0 \approx 0$ for $H \gg H_{irr}$) and the half-filled symbols to the metastable

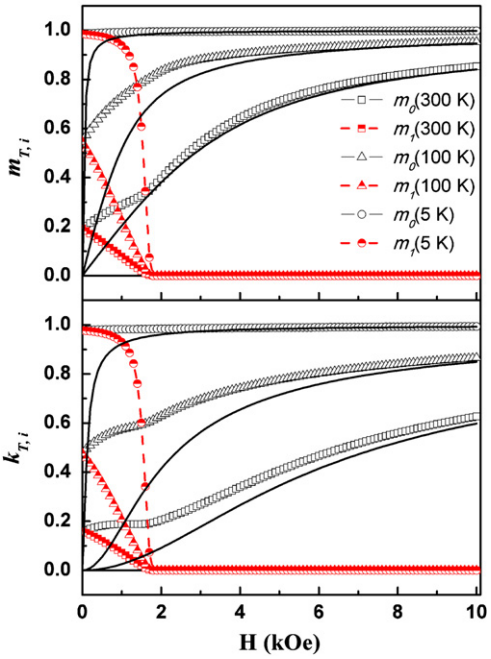

Fig. 9. $m_{T,i}$ and $k_{T,i}$ as a function of H. Thin continuous lines correspond to L_1 (top) and L_2 (bottom) functions plotted for comparison.

minimum labeled as "1". Circles, triangles and squares correspond to $T=5$, 100 and 300 K, respectively. The observed feature is similar for $m_{T,i}$ and $k_{T,i}$. At $H=0$, the statistical values of $k_{T,i}$ ($m_{T,i}$) are the same for both minima ($i=0$, 1) at each T. Increasing H, $m_{T,0}(H)$ and $k_{T,0}(H)$ increase because this minimum is oriented closer to the magnetic field direction, while the statistical average for $i=1$ begins to fall, and approaches 0 at $H\sim1.75$ kOe .In fact, when H achieves the irreversibility field, there exists only one minimum populated. However, the statistical average is still very useful, in order to consider the T-effect during the magnetization oscillation inside the $i=0$ minimum, as was considered in previous treatments [20,23,25]. In continuous lines we have plotted the L_1 and L_2 functions (Eq. 12a and b) which correspond to the SPM-model prediction for $m_{T,0}$ and $k_{T,0}$ respectively. As it is shown, there is a clear difference between $m_{T,0}(k_{T,0})$ with the SPM prediction at low fields, because L_1 (L_2) functions are null at $H=0$. When $H>H_A$, $m_{T,0}(k_{T,0})$ tends asymptotically to L_1 (L_2), as

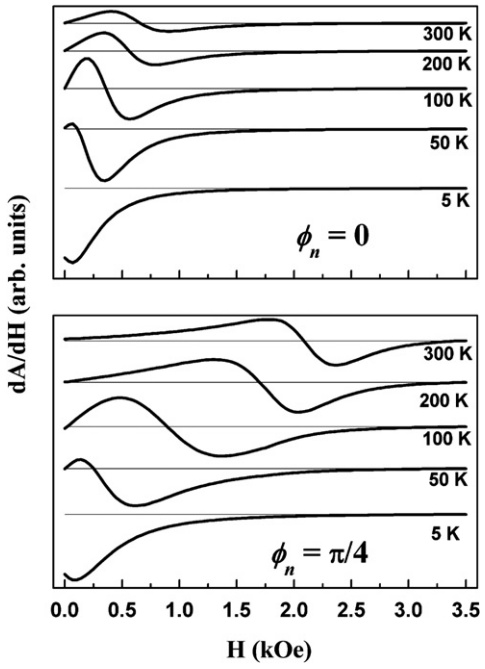

Fig. 10. Simulated FMR spectra as a function of T for $\varphi_n=0$ (top) and $\varphi_n=\pi/4$ (bottom).

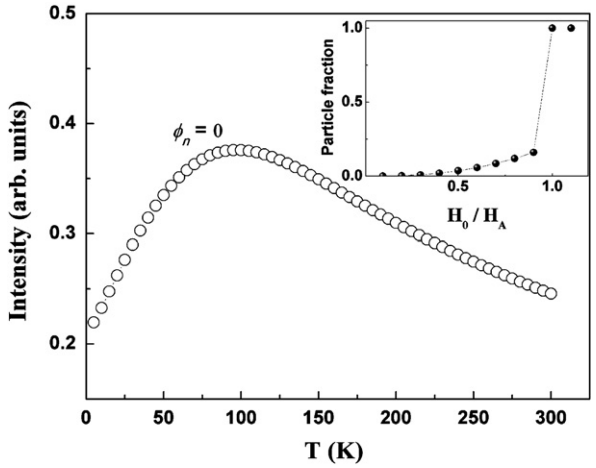

Fig. 11. Temperature evolution of the spectra intensity corresponding to $\varphi_n=0$ (associated to Fig. 10). The inset shows the particle fraction that contributes to the intensity as function of H_0/H_A.

expected. Also it is clear in Fig. 9 that the TFs decrease the statistical values $m_{T,i}(k_{T,i})$.

Fig. 10 presents numerical results for FMR spectra calculated at different temperatures between 300 K and 5 K. The top figure corresponds to the case $\varphi_n=0$ (H parallel to the easy axis), and the bottom one to $\varphi_n=\pi/4$ (H applied at 45° off the easy axis). A clear T-dependence of the spectra is observed. At low-T $H_{Aeff}>H_0$ and then the resonance condition cannot be fulfilled in both cases, observing only a "tail" of the resonance spectrum. As T is increased H_{Aeff} falls and the resonance condition can be reached. In this case the lineshapes become progressively more symmetrical and the resonance field increases. Fig. 10 corresponds to $H_A>H_0$; in the parallel configuration the system cannot achieve the resonance condition and then only a "tail" of the resonance is observed, depending on the linewidth $\Delta\omega/\gamma$. Fig. 11 shows the integrated intensity of FMR as function of temperature corresponding to $\varphi_n=0$ (top panel in Fig. 10). When H_{Aeff} becomes larger than H_0 the intensity decreases, because the resonance condition cannot be achieved. This behavior is frequently observed in powder samples, where the particles are randomly oriented. In order to explain this, we calculated the fraction of nanoparticles which contribute to the FMR signal for a randomly oriented system. The result is shown in the inset of Fig. 11 as function of H_0/H_A.

In general H_{Aeff} increases with decreasing T, thus, it is natural to expect a loss of intensity occurring when H_{Aeff} grows above H_0. Furthermore, under the condition $H_{Aeff}\approx H_0$ we can expect (see Fig. 2) *a decrease in the average resonance field* with a simultaneous *increase of the dispersion in resonance fields* (from the NP with easy axis oriented close to the applied field, to the NP with their axes nearly perpendicular to H), thus accounting for a simultaneous large linewidth [38]. These facts signal that the *intensity decrease* cannot be used as a feature that indicates the change from SPM to blocked regimes.

In Fig. 12 we present an ideal magnetic hysteresis loop, dispersion relation, and simulated FMR spectrum for comparison. The field is applied along the easy axis orientation ($\varphi_n=0$), and we consider a coherent inversion of the magnetization. The figure is divided into two columns, the left (right) one corresponds to low (high) anisotropy field. Each column is divided into three rows: the top one corresponds to the magnetization hysteresis loop, the middle one to the dispersion relation, and the bottom one to the FMR spectrum. In each row the full line corresponds to the DM case and the dashed line to IM. In the upper row we present a typical hysteresis behavior corresponding to a bi-stable magnetic system. The thick arrows indicate the path followed by the magnetization from the positive saturation situation to the negative one. Thin arrows indicate the opposite field sweep direction. In both cases we can observe the discontinuous behavior at $H=\pm H_A$ which reflects the passage of the magnetic moment from one energy minimum to the other. This is observed, also, in the dispersion relation [41]: it decreases linearly with H to zero (Eq. 6) and jumps suddenly joining the other dispersion curve. Strictly speaking, in a FMR experiment only the positive field region is usually explored, but the lines shown at negative values of H in the bottom panel illustrate and help to understand what happens in the DM and IM cases. The bottom row illustrates the FMR response. Following the thick arrows on the left column (low anisotropy) we observe that the system can achieve the resonance condition and then a "normal" spectrum is obtained (full line). A contrasting behavior is observed in the FMR response corresponding to high anisotropy (third row, right column). It is interesting to note that the zero-field absorption is not null if H_{Aeff} is close to H_0 in the scale of $\Delta\omega/\gamma$ (Eq. 7). When $H>H_{irr}$, the spectra are independent of the initial magnetization configuration.

In Fig. 13 we present numerical simulations to illustrate the DM and IM calculated FMR response which retains the essentials

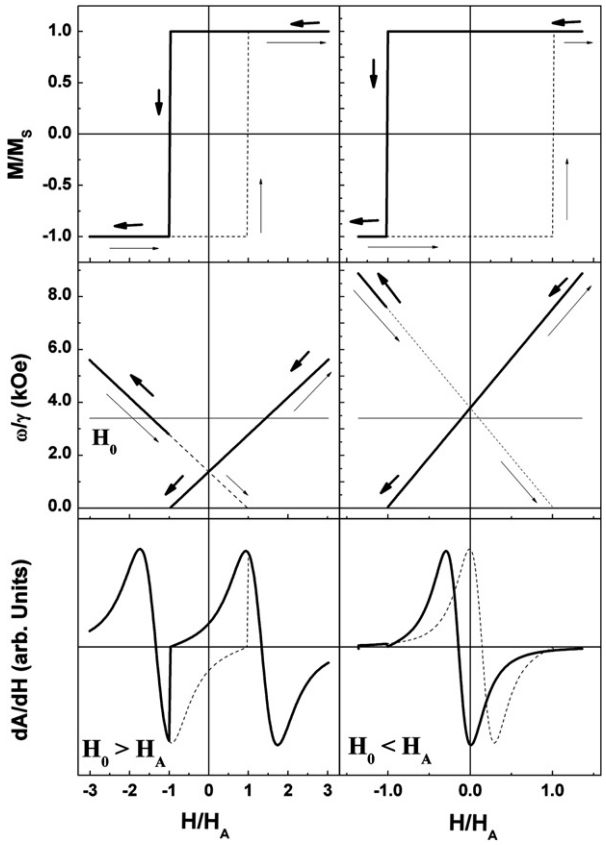

Fig. 12. Schematic representation of: square hysteresis loops (top), dispersion relations (middle), and FMR spectra (bottom). The left column corresponds to $H_{Aeff} < H_0$ and the right one to $H_{Aeff} > H_0$.

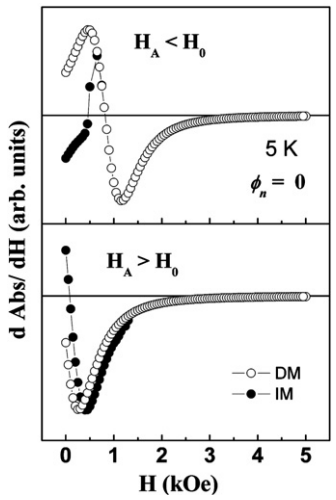

Fig. 13. Numerical simulation of the directly magnetized (DM) and inversely magnetized (IM) spectra for $H_A < H_0$ (top) and $H_A > H_0$ (bottom).

features observed in Fig. 8. The top (bottom) graph shows the $H_{Aeff} < H_0$ ($H_{Aeff} > H_0$) case, calculated for $\varphi_n = 0$, which corresponds to an anisotropy gap lower (higher) than H_0. Full dots correspond to the IM and the open ones to the DM. There are two "regions" in the spectra, one (at lower fields) in which an irreversible behavior is observed, and the other (at higher fields) which is reversible.

Note that the sign of the calculated FMR spectra at $H=0$ is opposite for DM and IM measurements, similar to what is observed experimentally (Fig. 8).

6. Conclusions

Finally, we want to remark that the FMR intensity loss is a phenomenon that is usually found when lowering T in NP systems [38,42,43]. The magnetic configuration of these particles often consists in an ordered core and a magnetic disordered shell at high temperatures. When T is lowered, the magnetic shell orders and induces in the magnetic core a larger anisotropy [42]. This produces a large increase on H_{Aeff} which reflects as a decrease of the FMR intensity and resonance field, and an increase in the linewidth [38].

We have presented experimental results and a model that describes how the FMR of nanoparticles is affected by thermal effects in a wide range of magnetic anisotropy. This work was based on the concept that the FMR of magnetic NP can be treated as traditional FMR experiments where TFs are considered. These TFs modify the minima population and influence the effective magnetization and anisotropy, which reflect in the resonance field and linewidth. The model agrees with the extrapolated behavior for low-temperatures and with the low-anisotropy regimes [20,23,25], giving a full description of the FMR response for intermediate cases which was not available. In addition, we could explain the FMR intensity loss observed in many cases at low temperatures, considering the increase of the effective anisotropy as responsible for this effect. The simulations closely resemble the observed features in the reversible and irreversible regions of the FMR for two typical low- and high-anisotropy systems of nanoparticles. The observed FMR irreversibility region is coherent with the one observed in magnetization measurements. We associate the characteristic measuring time in FMR with the field sweep rate and not with the inverse of the microwave frequency.

Acknowledgments

This work was partially supported by the Universidad Nacional de Cuyo, Conicet, and ANPCYT (Argentina) grants.

Appendix A. Minima region determination

In our model we referred to the statistical averages and the determination of each minimum region Ω_i. In order to determine each minimum region we combine two criteria, that correctly weighted, allow us to avoid some discontinuities in the average

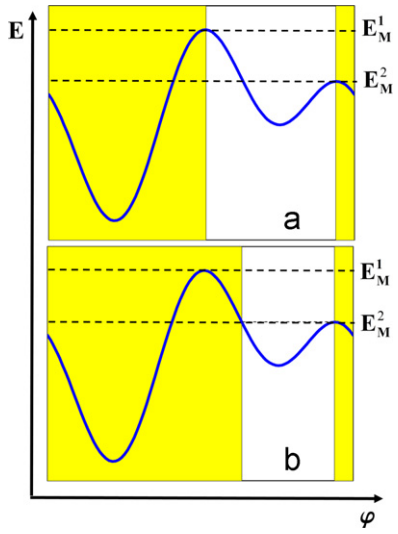

Fig. A1. Schematic representation of the minima energy region determination.

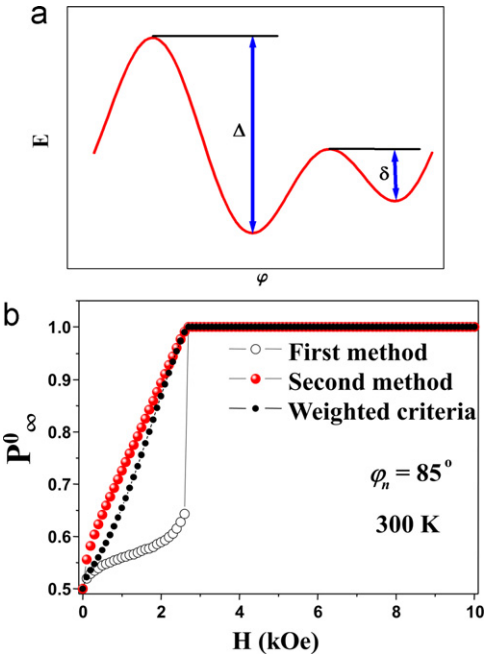

Fig. A2. (a) Schematic representation of the barrier energies δ and Δ. (b) Example of the equilibrium population as a function of H for the different methods (see text).

calculations of $k_{T,i}$ and $m_{T,i}$ in particular geometries. For a fixed θ value, the first method consists in sweeping the φ coordinate looking for the maxima (E_M^1 and E_M^2), which divide region Ω_0 from Ω_1 (in case a second minimum is present). This method is successful when φ_n is close to zero or in all orientations if $H \ll H_A$.

In the second method we associate to the second region, Ω_1, all points that have an energy value lower or equal than the maximum E_M^2. As an illustration and in order to clarify the concept, we define the second region as the one for all φ's that comply with $E(\theta,\varphi) < E_M^2$. In this way, the region Ω_1 becomes smaller than the other method. In Fig. A1 we schematize both methods. Grey (yellow online) region corresponds to Ω_0 and the white one to Ω_1. The top (a) and bottom (b) of Fig. A1 correspond to the first and the second methods, respectively.

Fig. A2(a) represents a hypothetical energy profile in which there are two energy barriers, labeled Δ and δ for the larger and smaller respectively. For a given energy surface we perform the averages (Eqs. (10) and (11)) over these regions using both methods. Each one of these results is finally weighted according to the following expression:

$$\begin{aligned} &<A> = <A_1> C_1 + <A_2> C_2 \\ &C_1 = \eta \\ &C_1 + C_2 = 1 \\ &\eta = 2\delta/(\delta+\Delta) \end{aligned} \tag{A1}$$

where the brackets $< >$ indicate an averaging process, A is the quantity considered, the subscript indicate the method used, C_1 and C_2 are weight factors calculated according to the barrier energies Δ and δ defined in Fig. A2(a).

In this way, when the magnetic field is low (compared to the anisotropy field) both minima are similar ($\eta \approx 1$), and the first criterion is privileged. Contrarily, when the energy values of both minima are very different, $\eta \approx 0$ and $C_2 \approx 1$ is dominant in eq. (A1) (second criterion is privileged). An example of the implementation of this criterion is shown in Fig. A2(b) where we present the equilibrium population P^0_∞. This picture illustrates the problems associated with each method, and how the weighted criterion eliminates the discontinuities.

References

[1] A.G. Gurevich, G.A. Melkov, Magnetization Oscillations and Waves, CRC Press, New York, 1996.
[2] P. Sharma, A. Gupta, K.V. Rao, F.J. Owens, R. Sharma, R. Ahuja, J.M. Osorio Guillen, B. Johansson, G.A. Gehring, Nature Materials 2 (2003) 673.
[3] C. Chappert, K. Le Dang, P. Beauvillain, H. Hurdequint, D. Renard, Physical Review B 34 (1986) 3192.
[4] S.E. Lofland, S.M. Bhagat, H.L. Ju, G.C. Xiong, T. Venkatesan, R.L. Greene, Physical Review B 52 (1995) 15058.
[5] A.N. Anisimov, M. Farle, P. Poulopoulos, W. Platow, K. Baberschke, P. Isberg, R. Wäppling, A.M.N. Niklasson, O. Eriksson, Physical Review Letters 82 (1999) 2390.
[6] A. Saib, D. Vanhoenacker-Janvier, I. Huynen, A. Encinas, L. Piraux, E. Ferain, R. Legras, Applied Physics Letters 83 (2003) 2378.
[7] N. Guskos, E.A. Anagnostakis, V. Likodimos, T. Bodziony, J. Typek, M. Maryniak, U. Narkiewicz, I. Kucharewicz, S. Waplak, Journal of Applied Physics 97 (2005) 024304.
[8] K. Shen, D.L. Tierney, T. Pietra, Physical Review B 68 (2003) 165418.
[9] A.S. Claye, N.M. Nemes, A. Jánossy, J.E. Fischer, Physical Review B 62 (2000) R4845.
[10] A.A. Kovalev, G.E.W. Bauer, A. Brataas, Physical Review B 75 (2007) 014430.
[11] M.I. Dolz, W. Bast, D. Antonio, H. Pastoriza, J. Curiale, R.D. Sánchez, A.G. Leyva, Journal of Applied Physics 103 (2008) 083909.
[12] L. Kraus, G. Infante, Z. Frait, M. Vázquez, Physical Review B 83 (2011) 174438.
[13] V. Boucher, D. Ménard, Physical Review B 81 (2010) 174404.
[14] M. Darques, J. Spiegel, J. De la Torre Medina, I. Huynen, L.J. Piraux, Journal of Magnetism and Magnetic Materials 321 (2009) 2055.
[15] S.P. Antonel, G. Jorge, O.E. Perez, A. Butera, G. Leyva, M.R. Negri, Journal of Applied Physics 110 (2011) 43920.
[16] E. De Biasi, R.D. Zysler, C.A. Ramos, M. Knobel, Journal of Magnetism and Magnetic Materials 320 (2008) e312.
[17] J.L. Dormann, D. Fiorani, E. Tronc, Advances in Chemical Physics 98 (1997) 283.
[18] R.S. de Biasi, T.C. Devezas, Journal of Applied Physics 49 (1978) 2466.
[19] W.F. Brown Jr., Micromagnetics, Interscience Publishers, New York, 1963.
[20] Y.L. Raikher, V.I. Stepanov, Physical Review B 50 (1994) 6250;
Y.L. Raikher, V.I. Stepanov, Soviet Physics Journal of Experimental and Theoretical Physics 75 (1992) 764.
[21] R.S. de Biasi, W.S.D. Folly, Physica B: Condensed Matter 321 (2002) 117.
[22] B.R. Pujada, E.H.C.P. Sinnecker, A.M. Rossi, C.A. Ramos, A.P. Guimarães, Physical Review B 67 (2003) 024402.
[23] E. De Biasi, C.A. Ramos, R.D. Zysler, Journal of Magnetism and Magnetic Materials 262 (2003) 235.
[24] E. Wajnberg, L.J. El-Jaick, M.P. Linhares, D.M.S. Esquivel, Journal of Magnetic Resonance 153 (2001) 69.
[25] R. Berger, J. Bissey, J. Kliava, H. Daubric, C. Estournès, Journal of Magnetism and Magnetic Materials 234 (2001) 535.
[26] T. Suominen, J. Raittila, T. Salminen, K. Schlesier, J. Lindén, P. Paturi, Journal of Magnetism and Magnetic Materials 309 (2007) 278.
[27] G. Ennas, A. Musinu, G. Piccaluga, D. Zedda, D. Gatteschi, C. Sangregorio, J.L. Stanger, G. Concas, G. Spano, Chemistry of Materials 10 (1998) 495.
[28] C. Antoniak, J. Lindner, M. Farle, Europhysics Letters 70 (2005) 250.
[29] A.V. Trunova, J. Linder, R. Meckenstock, M. Spasova, M. Farle, D. Ciuculescu, C. Amiens, B. Chaudret, M. Respaud, Journal of Magnetism and Magnetic Materials 321 (2009) 3502.
[30] Yu.A. Koksharov, S.P. Gubin, I.D. Kosobudsky, M. Beltran, Y. Khodorkovsky, A.M. Tishin, Journal of Applied Physics 88 (2000) 1587.
[31] H.K. Lachowicz, A. Sienkiewicz, P. Gierlowski, A. Slawska-Waniewska, Journal of Applied Physics 88 (2000) 368.
[32] J. De La Torre Medina, L. Piraux, J.M. Olais Govea, A. Encinas, Physical Review B 81 (2010) 144411.
[33] C. Kittel, Introduction to Solid State Physics, 8th edition, J. Willey & Sons, Hoboken, NJ, USA, 2005, pp. 379–383.
[34] G.V. Skrotskii, L.V. Kurbatov, in: S.V. Vonsovskii (Ed.), Ferromagnetic Resonance, Pergamon, Oxford, 1966.
[35] U. Netzelmann, Journal of Applied Physics 68 (1990) 1800.
[36] A.G. Roca, M.P. Morales, K. O'Grady, C.J. Serna, Nanotechnology 17 (2006) 2783.
[37] Xing-Hua Li, Cai-Ling Xu, Xiang-Hua Han, Liang Qiao, Tao Wang, Fa-Shen Li, Nano Express 5 (2010) 1039.
[38] E. De Biasi, R.D. Zysler, C.A. Ramos, H. Romero, Journal of Magnetism and Magnetic Materials 294 (2005) e83.
[39] E.C. Stoner, E. Wohlfarth, Philosophical Transactions of the Royal Society of London 240 (1948) 599.
[40] C.A. Ramos, E.C. Vassallo Brigneti, E. De Biasi, M. Vázquez, On the behavior of Ni Magnetic Nanowires as studied by FMR and the effect of 'blocking', Nanowires-Fundamental Research (2011) 333–364.
[41] C.A. Ramos, E. De Biasi, R.D. Zysler, E. Vassallo Brigneti, M. Vázquez, Journal of Magnetism and Magnetic Materials 316 (2007) e63.
[42] E. De Biasi, C.A. Ramos, R.D. Zysler, Physical Review B 65 (2002) 144416.
[43] E. De Biasi, C.A. Ramos, R.D. Zysler, H. Romero, Physica B 354 (2004) 286.